Emergence of robust precipitation changes across crop production areas in the 21st century

Maisa Rojas[a,b,1], Fabrice Lambert[b,c], Julian Ramirez-Villegas[d,e,f], and Andrew J. Challinor[d,e]

[a]Department of Geophysics, Universidad de Chile, 8370449, Santiago, Chile; [b]Center for Climate and Resilience Research, CR2, Universidad de Chile, 8370449, Santiago, Chile; [c]Department of Physical Geography, Pontificia Universidad Católica de Chile, 7820436, Santiago, Chile; [d]School of Earth and Environment, University of Leeds, LS2 9JT Leeds, United Kingdom; [e]CGIAR Research Program on Climate Change, Agriculture and Food Security, CIAT, 763537, Cali, Colombia; and [f]International Center for Tropical Agriculture, CIAT, 763537, Cali, Colombia

A warming climate will affect regional precipitation and hence food supply. However, only a few regions around the world are currently undergoing precipitation changes that can be attributed to climate change. Knowing when such changes are projected to emerge outside natural variability—the time of emergence (TOE)—is critical for taking effective adaptation measures. Using ensemble climate projections, we determine the TOE of regional precipitation changes globally and in particular for the growing areas of four major crops. We find relatively early (<2040) emergence of precipitation trends for all four crops. Reduced (increased) precipitation trends encompass 1–14% (3–31%) of global production of maize, wheat, rice, and soybean. Comparing results for RCP8.5 and RCP2.6 clearly shows that emissions compatible with the Paris Agreement result in far less cropped land experiencing novel climates. However, the existence of a TOE, even under the lowest emission scenario, and a small probability for early emergence emphasize the urgent need for adaptation measures. We also show how both the urgency of adaptation and the extent of mitigation vary geographically.

climate change | natural variability | precipitation | agriculture | CMIP5

Basic thermodynamics principles imply that global precipitation will increase in a warmer world, but with significant regional variations (1). The intensification of the hydrological cycle will result in a precipitation minus evaporation change pattern that has been termed the "rich-get-richer and poor-get-poorer" mechanism applicable over oceans (2). Due to large-scale atmospheric circulation and land/sea contrasts, regions that are already wet, such as the tropics and high latitudes, will become wetter, while dryer subtropical regions will become dryer (3).

Consistent precipitation changes are found in several regions in the two most recent simulation datasets of the Coupled Model Intercomparison Project (CMIP3 and CMIP5), which follow, to a large degree, the rich-get-richer expected pattern over oceans (4). Observational datasets indicate robust and statistically significant positive precipitation tendencies in parts of the Northern Hemisphere high latitudes (4), whereas mixed signals have been found in the tropics (5, 6).

Although the spatial patterns of changes have been widely investigated, few studies have addressed the question of timing [i.e., when the precipitation changes during the 21th century will consistently emerge outside the range of natural variability (7–9)]. Notably, no assessment of the timing of changes in precipitation with a focus on agricultural activities has been carried out to date (but refs. 10, 11). The time of emergence (TOE) is defined here as the moment when the magnitude of the ensemble mean precipitation change becomes greater than the uncertainty due to noise and natural variability (7) (*Methods*).

Although not the only relevant variable (12), precipitation variability plays a significant role in the agriculture sector, particularly as rainfed agriculture constitutes 60–95% of farmed land across the developing world (13). Crop-climate model projections indicate that reductions in agricultural productivity

of 0.5%, on average, are likely per every percentage point reduction in precipitation, although with large spatial variability (10, 14). In addition, global food supply is vulnerable because a large fraction of the global food production is concentrated in selected regions of the world (15, 16). Knowledge of the future precipitation trends in these regions is therefore of the utmost importance for the development and implementation of adequate adaptation strategies that will ensure future global food demand is met by production (17, 18). Here, we use a multimodel ensemble from the 21 CMIP5 (19) climate models that simulated all four representative concentration pathway (RCP) scenarios (20) (*Methods* and *SI Appendix*, Table S1) to identify key regions of the world where a precipitation TOE exists during the 21st century. We analyze both the annual mean and specific growing seasons and areas of the four major crops (wheat, soybean, rice, and maize), which, together, account for ~40% of total calorie intake globally (18). The TOE assessment by growing seasons helps identify regions in which 21st century crop production is expected to be permanently exposed to climate change-induced precipitation changes outside the range of natural variability, and may thus benefit from timely adaptation measures.

Results

The calculation of the TOE for the annual mean precipitation (Fig. 1) indicates that coherent patterns of increased (blue shading, 22–30% of global area) and decreased (red shading, 1–6% of global area) precipitation trends emerge in all four RCPs in several regions around the globe (*SI Appendix*, Table S2). Spatially, the TOE resembles the rich-get-richer pattern. The northern high latitudes, including Canada, the eastern United States, northern Europe, and Russia, exhibit a very early TOE of positive precipitation changes, some of them emerging as early as 2020 or

---

Significance

Using 21st century climate model projections we show that for many crop-producing regions, average precipitation will change by more than the long-term natural variability, even under a low-emission scenario. However, emissions compatible with the Paris Agreement can significantly reduce cropped land affected. We identify the regions where adaptation measures are most needed.
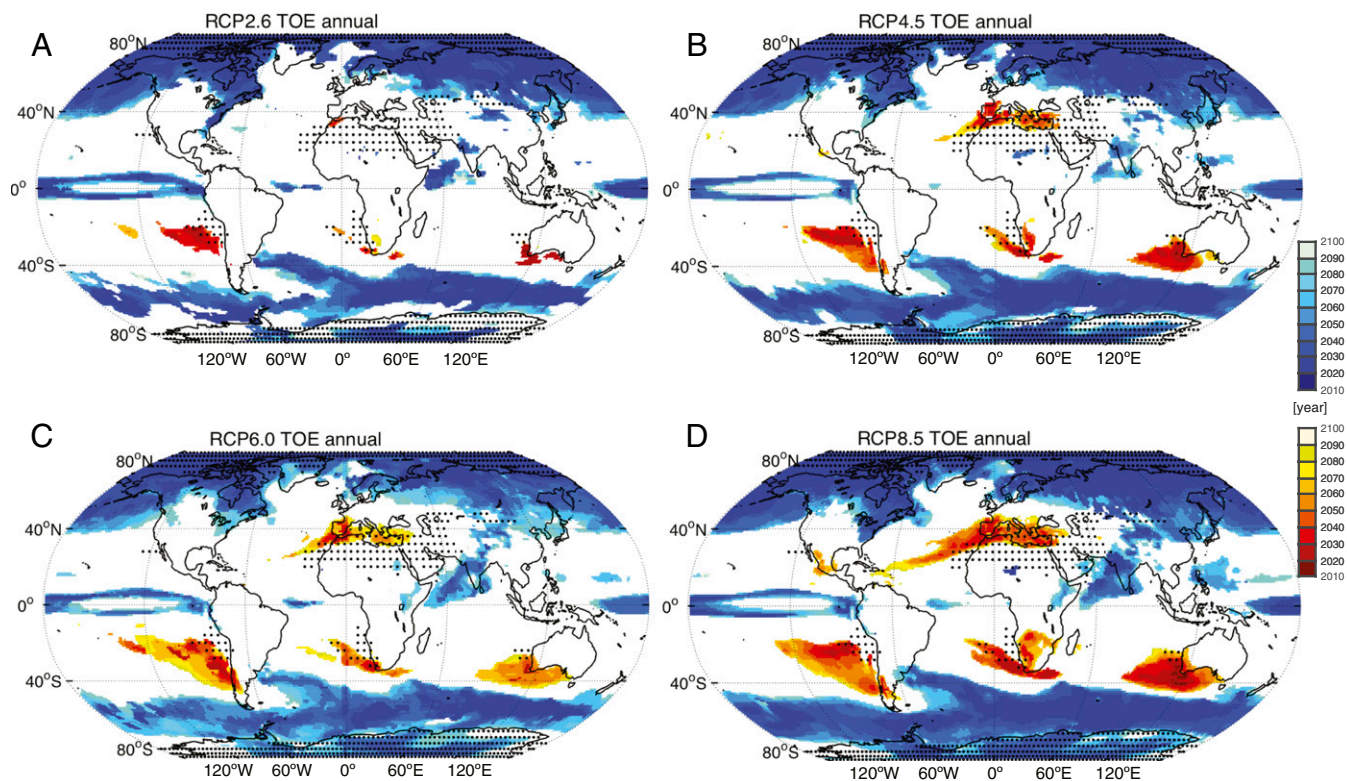

Fig. 1. TOE (year) of annual precipitation in RCP2.6 (*A*), RCP4.5 (*B*), RCP6.0 (*C*), and RCP8.5 (*D*). The red color scale is used for regions with a decrease in precipitation. The blue color scale is used for regions with an increase in precipitation. Stippling indicates climatological dry areas (below 50 mm·y⁻¹).

having already emerged (3). Southern high latitudes exhibit a similarly early TOE mostly over oceans. These changes are mostly explained by the thermodynamic increase in available humidity (21) and poleward-shifted storm tracks (22). In the tropics, our results indicate an increase of precipitation in the Intertropical Convergence Zone (ITCZ) also relatively early (<2030). Changes in the tropics are thought to be mainly driven by atmospheric circulation changes (ascent regions) (2, 23). Another important region with a positive precipitation change is India (<2030 for RCP8.5). As the ITCZ induces no TOE over either South America or Africa, this unique response of the Indian subcontinent may result from a positive response of the summer monsoon to climate change (ref. 24. and references therein).

Negative precipitation trends emerging outside natural variability occur in the Mediterranean region in all four RCPs in the early to midcentury, in western Mexico (only in RCP4.5 and RCP8.5) after the midcentury, and in three subtropical regions in the Southern Hemisphere around the midcentury in all four RCPs (Fig. 1), with all of them being Mediterranean-like climate regions. The drying trend in the subtropical dry regions is mainly thought to be a result of reduced water vapor in regions of subsidence (1). In both hemispheres, but especially in the three Southern Hemisphere regions, the drying occurs predominantly on the eastern side of the subtropical highs. This suggests a stronger advection of cool air masses from polar areas that increases the atmospheric stability in those regions and facilitates subsidence, as a result of a poleward expansion of the Hadley cell (22, 25), or strengthening of the circulation driven by thermodynamics of a warmer surface (26). Note that regions where a drying trend is expected all have significant natural variability in both observations and CMIP5 models (*SI Appendix*, Figs. S1–S3).

The northern high-latitude TOE pattern is mostly a result of the winter precipitation increase (*SI Appendix*, Fig. S4) and corresponds to a 10–20% precipitation increase at the TOE with respect to the 1986–2005 (historical baseline) level (*SI Appendix*, Fig. S5). Positive precipitation changes in the tropical regions (ITCZ and India) at the TOE correspond to changes of 20–30% and are due to both summer and winter contributions. The early drying (<2040) in the Mediterranean region corresponds to a 10–30% reduction. Seasonally, the winter precipitation decrease contributes to the signal in northern Africa and the Mediterranean Sea, whereas the summer drying is more important in southern Europe, including France (*SI Appendix*, Fig. S4). In the three Southern Hemisphere regions, drying at the TOE is 10–20% and the largest contribution to the drying is a decrease in winter precipitation.

Discussion

Changes in total available precipitation are a major risk for the global supply of food in the 21st century (10, 27). Recent climatic changes and climate variability have already put a stress on global food production (28). To estimate the potential implications of precipitation signal emergence for agriculture, we computed the TOE globally for the growing seasons in the production regions of the four major crops. Fig. 2 shows the TOE by growing season for the RCP8.5 (other RCPs are shown in *SI Appendix*, Figs. S6–S8), indicating at what time wheat-, soybean-, rice-, and maize-based farming systems can expect the regional climate to permanently leave the previous mean climate state and either settle around a new mean state or continue changing for the respective growing seasons. The majority of cropped areas for these crops do not show a TOE. Note that this does not mean that these regions do not have a precipitation trend, but just that the trend stays within the limits of natural variability during the time range of our analysis. Nevertheless, a globally significant percentage of current production will be affected by a TOE of precipitation changes (*SI Appendix*, Table S2). By doing the calculations for the specific growing season of
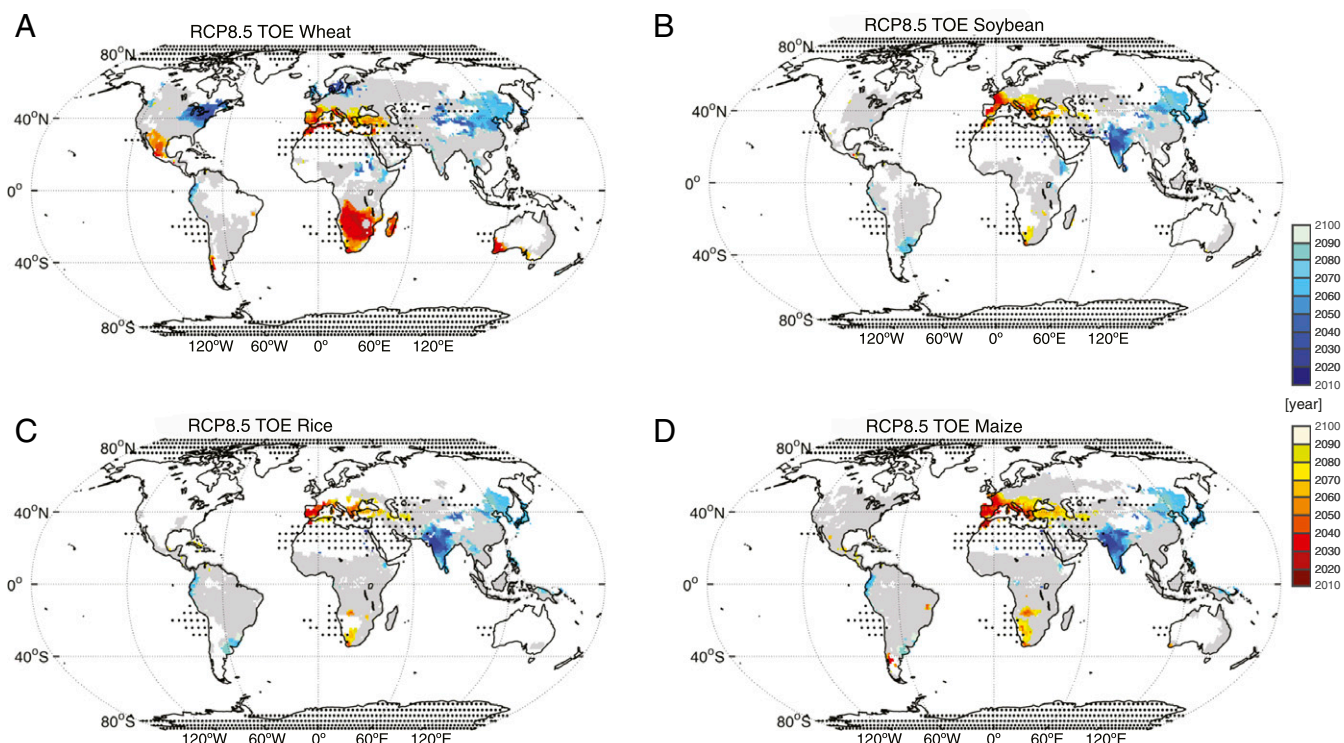
Fig. 2. TOE (year) of precipitation changes for RCP8.5 by growing season of wheat (*A*), soybean (*B*), rice (*C*), and maize (*D*). The red color scale is used for regions with a decrease in precipitation. The blue color scale is used for regions with an increase in precipitation. Gray indicates regions where a crop is grown, and all grid cells with harvested area by crop are shown. Stippling indicates climatological dry areas (below 50 mm·y⁻¹).

the crops, a number of differences from annual mean calculation are apparent. For example, an earlier decreasing precipitation TOE emerges in Mexico and southern Africa for wheat than in the annual mean calculation. In Europe, a decreasing precipitation TOE will affect a larger area of maize production compared with the annual mean calculation. Overall, for the RCP2.6 scenario (compatible with the 2 °C warming goal of the Paris Agreement) the affected areas by a TOE are greatly reduced.

Several agricultural regions in the Northern Hemisphere may experience a precipitation increase that will be permanently outside the current climate variability around midcentury (Fig. 2). Of particular importance are the present high-yielding regions in China, northern India, and the eastern United States. A key issue that emerges is thus the extent to which yield changes are expected in these regions. As a first approximation, we use a simple correlational analysis that shows, on average, agricultural yield will increase with precipitation (*SI Appendix*, Fig. S9). We may therefore expect an average increase in agricultural yield from regions with a positive TOE. While our trend analysis is not predictive and lacks the physiological detail necessary to explain the processes behind the yield–precipitation associations, it should capture the first-order yield–precipitation interactions in areas where robust precipitation changes are projected during the 21st century (*SI Appendix, Supplementary Information Text*).

The generally positive yield outcome in regions with increasing precipitation trends might be dampened by an important caveat: The clay, clay loam, and loam soils in these regions make them susceptible to floods with increased precipitation. By itself, increased precipitation does not necessarily increase the flood risk, since higher temperature will also enhance surface evapotranspiration. Therefore, in Fig. 3, we show the surface runoff changes and temperature at the TOE for RCP8.5. Runoff can be regarded as an indicator of topsoil saturation, and hence flooding. Temperature changes at the TOE are in the range of 0.5–2 °C. The

enhanced runoff in China, India, and the eastern United States suggests a higher frequency of flooding events in all three regions. Due to the relatively early TOE in these regions, temperature
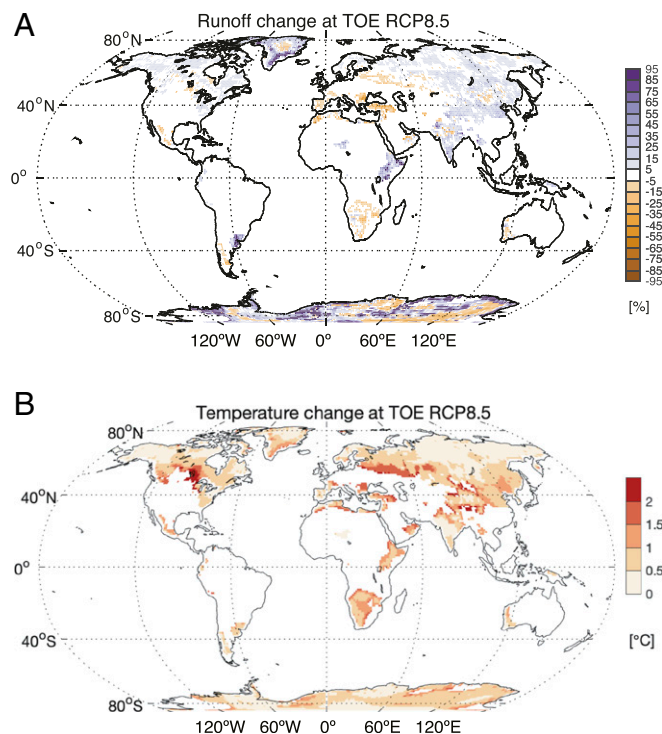

Fig. 3. Change at TOE compared with 1986–2005 for RCP8.5 of runoff (*A*) and temperature (*B*).

increases will be in the lower range, up to 1 °C. Potentially higher yields due to enhanced precipitation may therefore be negated by more flood events without investment in infrastructure and other adaptation measures. Similarly, currently dry and low-yielding regions in eastern Africa and southern India may experience wetter conditions in the future (*SI Appendix*, Table S3), which may also result in higher flood risk due to the low soil moisture absorption in these regions. Furthermore, over the past decades, wheat in the United States has increased, but under a cooling trend in the past decades (28), whereas for the TOE, important warming is expected in this region (Fig. 3*B*). On the other hand, yield in India has already shown decreases with recent positive temperature and precipitation trends (28).

High-yielding agricultural production in the Northern Hemisphere that may be impacted by reduced precipitation is concentrated in southwestern Turkey, Italy, southern France, the Iberian Peninsula, Morocco, and central Mexico. Areas with a TOE of decreasing precipitation in the Northern Hemisphere currently grow 75 million tons (11% of global production) of wheat and 53 million tons (8% of global production) of maize. In those countries, about 62% of wheat production and 69% of maize production will potentially be impacted in RCP8.5 (*SI Appendix*, Table S4).

In the Southern Hemisphere, some regions in Ecuador, Uruguay, Argentina, and Papua-New Guinea have a relatively late (>2060) TOE of increasing precipitation. The major feature in the Southern Hemisphere is the drying of the subtropical landmasses, particularly around the tip of South Africa, in central Chile, and in southern and southwestern Australia. In these last two regions, this represents approximately 50% and 30% of the country's wheat production, respectively. For southern Africa, existing evidence suggests that these changes, coupled with projected temperature changes, would reduce wheat and, to a lesser extent, maize production significantly (29). In these areas, 42 million tons of wheat (6% of global production) are currently produced, of which about 34% will be impacted in RCP8.5. *SI Appendix*, Tables S3 and S4 give detailed values by country.

Fig. 4 shows the cumulative percentage of production affected by a TOE of the four crops under RCP8.5. Overall, 20–30% of production is affected by precipitation increase, starting early in this century and quickly increasing after 2040. Precipitation decrease is found to affect mostly wheat- and maize-growing regions from 2030 onward. Note that although most agricultural regions do not experience a TOE, as identified by the CMIP5 simulations, production is not evenly distributed among all regions, and these regions might still be affected by varying precipitation trends (10, 16).
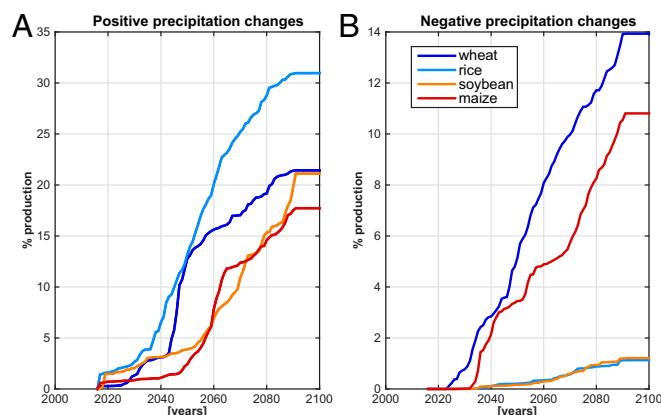
The TOEs of precipitation changes (positive and negative) found in this study allow identifying regions where precipitation changes are projected to move outside known natural variability within the 21st century, and hence can help to determine time scales at which policies and actions to adapt to climate change should be in place (e.g., refs. 11, 30). The spatial pattern of the TOE is robust to the exact method used to calculate the emergence (*Methods*), whereas the exact timing is more dependent on the baseline used, including a small probability of an early emergence of the signal (also ref. 9). In addition to precipitation, adaptation to climate change must clearly account for impacts from changes in temperature, evapotranspiration, and extreme events (among others); hence, many more regions than those found in this study are concerned. While only further analyses using detailed crop modeling approaches will help in the development of quantitative yield projections (which could be positive or negative), our TOE analysis identifies the spatial and temporal ranges where these studies may be most urgently needed. In all likelihood, the positive and negative precipitation trends identified in this study will require regional investment in adaptation, although a more complete diagnosis of productivity and cropped area change at the TOE than we have performed here is warranted to guide such adaptation investments. Flood and drought intensification may require governments to invest in infrastructure resilience, and may require farmers to reconfigure their cropping systems toward growing more drought-tolerant crops (e.g., from maize to sorghum or millets). One result of this analysis we would like to stress in particular is that a TOE was found for most of the regions even in the low-emission RCP2.6 scenario, highlighting the need for adaptation even under stringent mitigation scenarios. However, in comparison with higher emission scenarios, pursuing emission cuts compatible with the Paris Agreement can significantly reduce the potential impacts of climate change on crops.

Methods

Calculation of TOE. A total of 21 CMIP5 models were used in this study, analyzing simulations of the historical and all four RCP scenario experiments. Most of the models comprise more than one and up to 25 ensemble members in their experiments (*SI Appendix*, Table S1). The TOE is the ratio between the climate change precipitation signal and the estimated natural variability and uncertainty and noise, calculated as described by Giorgi and Bi (7). This method accounts for model spread, assuming that the models span the possible range of climate responses. All models were linearly interpolated onto a common 1° × 1° grid. A conservative interpolation leads to qualitatively the same result (*SI Appendix*, Fig. S10). At each grid point, the mean 20th century precipitation is calculated as the mean of the 1986–2005 period. We consecutively calculate the model mean precipitation change using a 20-y running window of the difference with respect to the base period. The total uncertainty due to intermodel spread and internal multidecadal variability is calculated by adding the variance of each model with respect to the multimodel ensemble mean (intermodel component) to the variance of each model with respect to its own ensemble mean (decadal component). Giorgi and Bi (7) emphasize that in this procedure, the information is most affected by the models with a larger number of realizations; however, as in their work, the internal decadal variability in this study is much smaller than the uncertainty due to intermodel spread. After having defined the measures of signal and noise, the running temporal average of the 20-y ensemble mean change of precipitation and associated total variance of the 20-y changes are calculated. For each grid cell, we thus obtain a yearly time series of mean 20-y changes and uncertainty, where, for each year of the time series, the running average is taken over the previous 10 y and following 10 y. Once the time series of ensemble mean changes and corresponding total standard deviation (STD) are calculated, the TOE is defined as the time at which the magnitude of the mean change becomes greater than that of the STD and remains so thereafter. To test the robustness of results, we also calculated the TOE as the time when the precipitation in each individual model moves outside the range of its own variability, measured by the STD of the baseline period. A model mean TOE is calculated as the mean of the individual TOE at grid points where at least 70% of models have a TOE. The results are qualitatively the same, and *SI Appendix*, Fig. S11

Fig. 4. Cumulative percentage of global production of four major crops affected by positive (*A*) and negative (*B*) precipitation changes under RCP8.5.

shows the result for the RCP8.5. To evaluate the less probable outcomes, *SI Appendix*, Fig. S11 also includes the 10th and 90th percentiles of the TOE calculated by this second method. Note that this shows that there is a small probability for a very early TOE over the same geographical areas that were identified with the conventional definition of TOE. Furthermore, using large-ensemble simulations, Zhang and Delworth (9) find that over the period 2000–2009, more than a third of the globe already shows a distinguishable precipitation shift compared with the 1950–1999 period, further corroborating our results.

Given that there are a number of time lengths important for agriculture, the sensitivity of our results to the lengths of the baseline period used was also explored. The 20-y baseline choice is justified from a signal-to-noise perspective. On the other hand, in a 5-y period, a complete El Niño Southern Oscillation (ENSO), for example, or the transition from a positive to negative (or vice versa) ENSO phase can be captured, whereas in a 10-y period, two ENSO phases can be captured. However, a 20-y period is likely to be a better representation of the long-term behavior of the production/food system, which is our interest.

We have rerun the analysis for different time periods: 5-y and 10-y baseline lengths. For example, a 5-y filter is used to reflect the importance of yield fluctuations at short time scales (e.g., consecutive crop failures). The results show a similar spatial pattern but, overall, a delay in the TOE by 5–10 y. This is due to the larger interannual variability at shorter time scales (*SI Appendix*, Fig. S12).

Model Validation. The correct calculation of the TOE depends on the ability of models to reproduce natural variability. To account for model biases, we compare natural and simulated precipitation variability using the coefficient of variation. Variability of natural and simulated precipitation was evaluated by calculating the coefficient of variation over the period 1901–2005 in the Climatic Research Unit (CRU) TS3.3 dataset (31) and full CMIP5 monthly data, respectively (*SI Appendix*, Fig. S1). Both datasets show good spatial agreement, although the CMIP5 ensemble tends to underestimate the variance in some areas, particularly in agricultural regions. In both the data and models, the interannual variability represents 60–80% of the total variance (*SI Appendix*, Fig. S2). The slight underestimation of the total variance in the models seems to stem mainly from the models' lower decadal variability compared with the CRU data (*SI Appendix*, Fig. S3). However, as intermodel spread is likely larger than natural variability, our TOE calculation will represent an upper bound of the true time at which precipitation changes may emerge above/below natural

variability of the historical climate. Finally, a low-pass filter was constructed to separate the decadal component of this variance, and a high-pass filter to separate the interannual component of the variance, for the annually averaged CRU and CMIP5 data. *SI Appendix*, Fig. S13 shows the distribution of the differences between the coefficients of variation of each model and CRU for three latitudinal bands, indicating that the models have lower variance compared with the observations, especially at middle to high latitudes.

Agriculture Calculations. The global analysis of TOE for agriculture was performed using the same procedures as for the annual mean, but for the growing seasons and global harvested areas of four crops. Our analysis focused on wheat, soybean, rice, and maize, which, together, contribute to *ca.* 40% of daily per capita caloric intake across the globe (32). Crop calendars were gathered from the study of Elliott et al. (33), in which a global crop calendar for each crop was derived through harmonization of existing global cropping calendar datasets (34–36). Harvested areas and production data were gathered from a study by Monfreda et al. (15). Crop calendar, harvested area, and production data were aggregated to the analysis grid (1° × 1°) and then used to define where and when (i.e., the planting-to-harvest periods) to compute mean precipitation and then conduct the TOE analysis. Gridded production data were then used, together with the results of the TOE analysis, to compute the total and proportional amounts of area affected by detectable positive or negative precipitation trends. In Fig. 2, we only plotted grid cells that had an area of at least 1% of the harvested crop. For calculations of *SI Appendix*, Tables S3 and S4, we used values of all grid cells, without considering a threshold.

To understand possible yield implications of projected seasonal precipitation changes at the TOE, the following analysis was conducted. The meta-analysis database from Challinor et al. (10) was used to identify the extent of variation in the yield response, given precipitation change scenarios. We refrain from a more complex analysis since the primary aim of this study is to detect robust precipitation changes in areas and times at which crops are grown, rather than to estimate potential effects on crop productivity, growing areas, or production; to assess the climate change signal on crop productivity projections; or to understand with sufficient detail the processes involved in potential yield changes. Future studies could build upon our analysis to develop a more detailed understanding of yield implications at the TOE.

1. Allan RP, et al. (2014) Physically consistent responses of the global atmospheric hydrological cycle in models and observations. *Surv Geophys* 35:533–552.
2. Held IM, Soden BJ (2006) Robust responses of the hydrological cycle to global warming. *J Clim* 19:5686–5699.
3. Collins M, et al. (2013) Long-term climate change: Projections, commitments and irreversibility. *Climate Change 2013: The Physical Science Basis*, Contribution of Working Group I to the Fifth Assessment Report of the Intergovernmental Panel on Climate Change, eds Stocker TF, et al. (Cambridge Univ Press, Cambridge, United Kingdom).
4. Hartmann DL, et al. (2013) Observations: Atmosphere and surface. *Climate Change 2013: The Physical Science Basis*, Contribution of Working Group I to the Fifth Assessment Report of the Intergovernmental Panel on Climate Change, eds Stocker TF, et al. (Cambridge Univ Press, Cambridge, United Kingdom).
5. Allan RP, Soden BJ, John VO, Ingram W, Good P (2010) Current changes in tropical precipitation. *Environ Res Lett* 5:25205–25208.
6. Byrne MP, Pendergrass AG, Rapp AD, Wodzicki KR (2018) Response of the intertropical convergence zone to climate change: Location, width, and strength. *Curr Clim Change Rep* 4:355–370.
7. Giorgi F, Bi X (2009) Time of emergence (TOE) of GHG-forced precipitation change hot-spots. *Geophys Res Lett* 36:653–656.
8. Mahlstein I, Portmann RW, Daniel JS, Solomon S, Knutti R (2012) Perceptible changes in regional precipitation in a future climate. *Geophys Res Lett* 39:L05701.
9. Zhang H, Delworth TL (2018) Robustness of anthropogenically forced decadal precipitation changes projected for the 21st century. *Nat Commun* 9:1150.
10. Challinor AJ, et al. (2014) A meta-analysis of crop yield under climate change and adaptation. *Nat Clim Chang* 4:287–291.
11. Rippke U, et al. (2016) Timescales of transformational climate change adaptation in sub-Saharan African agriculture. *Nat Clim Chang* 6:605–609.
12. Schlenker W, Roberts MJ (2009) Nonlinear temperature effects indicate severe damages to U.S. crop yields under climate change. *Proc Natl Acad Sci USA* 106:15594–15598.
13. Wani SP, Rockstrom J, Oweis T, eds (2009) *Rainfed Agriculture: Unlocking the Potential* (CAB International, Cambridge, MA).
14. Ray DK, Gerber JS, MacDonald GK, West PC (2015) Climate variation explains a third of global crop yield variability. *Nat Commun* 6:5989.
15. Monfreda C, Ramankutty N, Foley JA (2008) Farming the planet: 2. Geographic distribution of crop areas, yields, physiological types, and net primary production in the year 2000. *Global Biogeochem Cycles* 22:GB1022.
16. Porter JR, et al. (2014) Food security and food production systems. *Climate Change 2014: Impacts, Adaptation, and Vulnerability. Part A: Global and Sectoral Aspects*, Contribution of Working Group II to the Fifth Assessment Report of the Intergovernmental Panel on Climate Change, eds Field CB, et al. (Cambridge Univ Press, Cambridge, United Kingdom), pp 485–533.
17. Springmann M, et al. (2016) Global and regional health effects of future food production under climate change: A modelling study. *Lancet* 387:1937–1946.
18. FAOSTAT (2013) Agriculture data. Available at http://www.fao.org/faostat/en/#data. Accessed February 1, 2019.
19. Taylor KE, Stouffer RJ, Meehl GA (2012) An overview of CMIP5 and the experiment design. *Bull Am Meteorol Soc* 93:485–498.
20. van Vuuren DP, Edmonds JA, Kainuma M, Riahi K, Weyant J (2011) A special issue on the RCPs. *Clim Change* 109:1–4.
21. Seager R, Naik N, Vecchi GA (2010) Thermodynamic and dynamic mechanisms for large-scale changes in the hydrological cycle in response to global warming*. *J Clim* 23:4651–4668.
22. Wu Y, Ting M, Seager R, Huang H-P, Cane MA (2010) Changes in storm tracks and energy transports in a warmer climate simulated by the GFDL CM2.1 model. *Clim Dyn* 37:53–72.
23. Sobel AH, Camargo SJ (2011) Projected future seasonal changes in tropical summer climate. *J Clim* 24:473–487.
24. Chaturvedi RK, Joshi J, Jayaraman M, Bala G (2012) Multi-model climate change projections for India under representative concentration pathways. *Curr Sci* 103:1–12.
25. Scheff J, Frierson DMW (2012) Robust future precipitation declines in CMIP5 largely reflect the poleward expansion of model subtropical dry zones. *Geophys Res Lett* 39: 143–146.
26. Quan X-W, Diaz H, Hoerling MP (2004) Change of the tropical Hadley cell since 1950. *The Hadley Circulation: Present, Past, and Future.* Advances in Global Change Research 21, eds Diaz HF, Bradley RS (Springer, Dordrecht, The Netherlands) pp 85–120.
27. Lobell DB, Tebaldi C (2014) Getting caught with our plants down: The risks of a global crop yield slowdown from climate trends in the next two decades. *Environ Res Lett* 9: 74003–74009.
28. Lobell DB, Schlenker W, Costa-Roberts J (2011) Climate trends and global crop production since 1980. *Science* 333:616–620.
29. Estes LD, et al. (2013) Projected climate impacts to South African maize and wheat production in 2055: A comparison of empirical and mechanistic modeling approaches. *Glob Change Biol* 19:3762–3774.
30. Challinor AJ, Koehler AK, Ramirez-Villegas J, Whitfield S, Das B (2016) Current warming will reduce yields unless maize breeding and seed systems adapt immediately. *Nat Clim Chang* 6:954–958.

31. Harris I, Jones PD, Osborn TJ, Lister DH (2014) Updated high-resolution grids of monthly climatic observations–The CRU TS3.10 dataset. *Int J Climatol* 34:623–642.
32. Khoury CK, et al. (2014) Increasing homogeneity in global food supplies and the implications for food security. *Proc Natl Acad Sci USA* 111:4001–4006.
33. Elliott J, et al. (2015) The global gridded crop model intercomparison: Data and modeling protocols for phase 1 (v1.0). *Geosci Model Dev* 8:261–277.
34. Sacks WJ, Deryng D, Foley JA, Ramankutty N (2010) Crop planting dates: An analysis of global patterns. *Glob Ecol Biogeogr* 19:607–620.
35. Portmann FT, Siebert S, Döll P (2010) MIRCA2000—Global monthly irrigated and rainfed crop areas around the year 2000: A new high-resolution data set for agricultural and hydrological modeling. *Global Biogeochem Cycles* 24:GB1011.
36. Waha K, van Bussel LGJ, Müller C, Bondeau A (2011) Climate-driven simulation of global crop sowing dates. *Glob Ecol Biogeogr* 21:247–259.

Rojas et al.